Targeted covalent inhibition of prolyl oligopeptidase (POP): discovery of sulfonylfluoride peptidomimetics

Salvador Guardiola,[a] Roger Prades,[b] Laura Mendieta,[b] Arwin J. Brouwer,[c] Jelle Streefkerk,[c] Laura Nevola,[a] Teresa Tarragó,[b] Rob M. J. Liskamp,[*c,d] Ernest Giralt[*a,e]

[a]Institute for Research in Biomedicine (IRB Barcelona), The Barcelona Institute of Science and Technology, Baldiri Reixac, 10, 08028 Barcelona, Spain
[b]Iproteos, S.L., Barcelona Science Park, Baldiri Reixac 10, 08028 Barcelona, Spain
[c]Department of Chemical Biology and Drug Discovery, Utrecht Institute for Pharmaceutical Sciences, Faculty of Science, Utrecht University, 3508 TB Utrecht, The Netherlands
[d]School of Chemistry, University of Glasgow, University Avenue, Glasgow G12 8QQ, UK
[e]Department of Inorganic and Organic Chemistry, University of Barcelona, Spain

ernest.giralt@irbbarcelona.org, Robert.Liskamp@glasgow.ac.uk

*Lead contact: Ernest Giralt

Summary

Prolyl oligopeptidase (POP), a serine protease highly expressed in the brain, has recently emerged as an enticing therapeutic target for the treatment of cognitive and neurodegenerative disorders. However, most reported inhibitors suffer from short duration of action, poor protease selectivity and low blood-brain barrier (BBB) permeability, which altogether limit their potential as drugs. Here we describe the structure-based design of the first irreversible, selective and brain-permeable POP inhibitors. At low nanomolar concentrations, these covalent peptidomimetics produce a fast, specific and sustained inactivation of POP, both *in vitro* and in human cells. More importantly, they are >1000-fold selective against two family-related proteases (DPPIV and FAP) and display high BBB permeability, as shown in both lipid membranes and MDCK cells.

Introduction

As tools for chemical biology, peptides often show low permeability across biological barriers and rapid dissociation rates, two factors that limit their potential to target intracellular proteins (Huhn et al., 2016). On the other hand, small molecules can achieve higher potency and permeability, but they have sometimes proved insufficient for the selective manipulation of proteins that share high analogy with other members of the family, such as kinases and proteases. These issues have stimulated research (Baillie, 2016) on the use of modified peptides (peptidomimetics) as an alternative class of covalent inhibitors able to encompass two main components: i) better selectivity, by retaining the main features of peptides—i.e. topological diversity and selective recognition of the target; and ii) high affinity, by incorporating mild electrophiles and transforming them into covalent inhibitors.

Here we focused this approach on the inhibition of prolyl oligopeptidase (POP), an 81-kDa cytosolic protease that is prominently expressed in the brain with the capacity to hydrolyze post-proline bonds of small peptides (Yoshimoto et al., 1983). Besides its enzymatic function, POP plays important roles in neurogenesis, brain plasticity and memory formation (Höfling et al., 2016), although the exact mechanisms are not fully known. Being a highly dynamic protein (López et al., 2016), recent studies point to the involvement of POP in protein-protein interactions (PPIs) with other partners such as GAP43, a protein involved in neuronal function (Di Daniel et al., 2009), and α-synuclein, an intrinsically disordered protein associated with Parkinson's disease (Brandt et al., 2008). In agreement with these findings, POP was shown to accelerate α-synuclein aggregation *in vitro* and in cell cultures (Savolainen et al., 2015), thus providing an explanation to the co-localization of both proteins in the brain of Parkinson's disease (PD) patients (Hannula et al., 2013).

Due to its therapeutic potential, numerous compounds have been developed as POP inhibitors and tested in preclinical settings. Notably, in mouse models of PD, they have been able to accelerate the clearance of aggregated α-synuclein in the brain and, more importantly, to restore the motor behavior that is impaired as a result of the disease (Svarcbahs et al., 2016). Also recently, POP inhibitors have shown to significantly improve the cognitive symptoms affected by schizophrenia in mice (Prades et al., 2017). Despite these promising results, POP inhibitors have failed to succeed in clinical trials, two main factors limiting their success: poor selectivity against related prolyl peptidases (causing side effects) and lack of permeability through the blood-brain barrier (BBB), which limits their distribution inside the central nervous system (CNS) (López et al., 2013). Here we address these key issues through the design and characterization of a new class of covalent POP inhibitors.

Structure-guided design of irreversible POP inhibitors

In recent years, numerous POP inhibitors have been reported from a variety of scaffolds such as natural products (Tarrago et al., 2007), small molecules (Mariaule et al., 2016), peptides and peptidomimetics (López et al., 2013). Some of them feature C-terminal reactive functionalities, such as aldehyde, hydroxymethyl ketone or nitrile, which covalently bind to the hydroxyl group of the catalytic serine (Ser554). Structure-activity studies have shown that these covalent inhibitors are more potent and effective than their non-covalent analogs (Juillerat-Jeanneret, 2008). However, these molecules form a transient covalent bond with the enzyme that is hydrolyzed after a short time, thus regaining enzymatic activity. Thus, a main goal in our structure-based design was to endow our molecules with longer target residence times, as well as improved selectivity and membrane permeability.

The active site of POP comprises three well-defined cavities: S1, S2 and S3 (Schechter and Berger, 1967) that accommodate the peptide substrate and place the C-terminal prolyl carboxylate in close proximity to the catalytic Ser554 (Figure 1A). From a structural perspective, S1 and S2 are narrow cavities that tightly fit around the substrate proline rings and account for the high specificity of the enzyme (Fülöp et al.,

1998). The S3 pocket, in contrast, is a larger cavity flanked by hydrophobic residues Phe173, Met235, Cys255, Ile591 and Ala594. For the design of our shape-complementary inhibitors, we have divided the molecules into three parts (P1, P2 and P3) and followed a rational strategy, considering some of the best pharmacophores for potency and selectivity, together with a new electrophilic proline derivative.

At position P3, POP inhibitors often present a single phenyl ring, such as the Cbz group of ZPP (Yoshimoto et al., 1985). Instead of the carbamate of the Cbz, a three-carbon aliphatic chain—as in KYP-2047 (Venäläinen et al., 2006)—has been found optimal for POP inhibition (Figure 1A and 1B). However, careful structural analysis reveals that the S3 pocket is large enough to accommodate bulkier aromatic residues, such as Fmoc (Li et al., 1996), which can provide selectivity against other prolyl peptidases. For this purpose, we have included in our designs a fluorinated gallic acid derivative (4-(benzyloxy)-3,5-difluorobenzoyl, or BdFB), which in our hands provided not only high selectivity, but also extended microsomal stability and high lipid permeability (Giralt et al., 2014). At position P2, L-proline or close analogues are optimal for activity (López et al., 2011). Here, with the aim to enhance the drug-like properties of our inhibitors, we have further explored the introduction of small substituents (-F, $-F_2$, $-CH_3$ or $-CF_3$) at position 4 of the proline ring (Figure 1C).

Finally, at position P1 we have conveniently replaced the C-terminal carboxylate of the natural substrate with a mildly reactive electrophile, such as a sulfonyl fluoride moiety. Upon binding, this group is intended to form a stable covalent bond with the catalytic Ser554 of the enzyme, thus blocking its activity. In contrast to other more reactive warheads, sulfonyl fluorides have an adequate balance of biocompatibility, aqueous stability and protein reactivity (Narayanan and Jones, 2015), and have found significant use as probes in chemical biology. Peptidyl sulfonyl fluorides, in particular, have been developed as chymotrypsin (Brouwer et al., 2011) and proteasome (Dubiella et al., 2014) inhibitors, among other applications, showing therapeutic efficacy and safety when administered in mice (Tschan et al., 2013). All in all, with the triple objective of achieving high potency, selectivity and CNS permeability, we sought to condense this intricate structure-activity data into a peptidomimetic scaffold that combines optimal P2 and P3 moieties with a unique prolylsulfonyl fluoride warhead, leading to a total of 15 potential inhibitors (Table 1).

Special attention was devoted to those inhibitors bearing the BdFB P3 group, as this moiety is much bulkier than the gold standards Cbz and phenylpropyl. However, covalent docking calculations revealed that these compounds can adopt a very similar pose to that reported for reversible inhibitors ZPP and KYP-2047 (Figure 3A) (Kaszuba et al., 2012). As a differential trait, the larger fluorinated BdFB moiety is able to occupy most of the S3 cavity, resulting in extended π-π contacts with F173 and W595 of POP. On the other hand, the sulfonyl group at position P1, despite being larger than the natural amide, is well fitted between Asn555 and His680, and provides an optimal binding geometry towards Ser554. The flexible methylene group connecting the sulfur

atom to the pyrrolidine ring also facilitates the accommodation of the electrophile in front of the Ser554 side chain, thus enabling the covalent binding to occur.

Sequential synthesis yields highly potent POP inhibitors

The synthesis of the proline warhead was accomplished by starting from the natural precursor L-prolinol (Figure S1A). The hydroxyl group was oxidized in two steps to the sodium sulfonate, which was fluorinated to the corresponding sulfonyl fluoride. For this reaction, the use of XtalFluor-M (L'heureux et al., 2010) provided a cleaner crude product and a higher yield (76%) compared to other fluorinating agents such as DAST and XtalFluor-E (13% and 69% yield, respectively). Once the warhead was obtained, a divergent strategy was followed to sequentially couple the respective P2 and P3 groups (Figure S1B). A single purification step, at the end of the synthesis, afforded the final compounds in a milligram scale.

For evaluation and quantification of enzyme inhibition, a fluorometric assay was set up using recombinant human POP. To allow for comparison, IC_{50} values were determined at regular time points during the linear phase of the inhibition process (Figure S2). Although dependent on the preincubation time, IC_{50} values are a useful metric to compare the potency of a given set of inhibitors, since their full kinetic characterization (see below) is more laborious and time-consuming. As expected from the rational design, all molecules had strong potencies in the low nanomolar range (Table 1). Derivatization of position 4 of the P2 proline ring (R1, R2), meant to enhance the selectivity and membrane permeability of the inhibitors, was well-tolerated (inhibitors **11** and **18**). Notably, the BdFB moiety used at P3 resulted in highly potent compounds (**17**-**20**).

Sulfonyl fluoride peptidomimetics show high BBB permeability

In addition to potency, it is imperative that POP inhibitors cross the BBB to enter the brain tissue, a criterion that peptidomimetic drugs often fail to meet (López et al., 2013). This is not surprising given that the BBB—a highly specialized and complex vascular system—prevents most (>98%) drugs from reaching the CNS (Pardridge, 2005). To address this issue, we studied the transport of our compounds in the PAMPA assay, in which a lipid brain extract mimics the composition of the BBB, resulting in a convenient method to evaluate the transport of compounds by passive diffusion (Di et al., 2003). Reassuringly, high permeability values were obtained for all three families of compounds ($P_e > 10^{-5}$ cm s^{-1}, see Table 1), in the same range as propranolol, a highly permeable CNS-active drug used as positive control. In particular, transport was increased upon fluorination of the P2 proline ring; in contrast, the introduction of lipophilic groups (CH_3 and CF_3) led to membrane retention and a slight decrease in permeability. To further validate these results, also taking the effect of active transport and efflux pumps into account, we evaluated the absorptive transport through a monolayer of MDCK cells, which is a more relevant model for the prediction of BBB permeability (Wang et al., 2005). Again, all inhibitors achieved excellent transport rates, in some cases higher than the FDA-approved drug metoprolol (Figure 2A). Only

the BdFB compounds showed slightly lower values due to retention in lipids, as also shown in the PAMPA.

High-affinity covalent binding is not compromised by off-target effects

In addition to POP, the S9 family of serine-proteases holds other proline-specific peptidases, such as fibroblast activation protein (FAP) and dipeptidyl peptidase IV (DPPIV), which also hydrolyze proline-containing peptide hormones and neuropeptides. While DPPIV is exclusively an exopeptidase, FAP also shares equivalent endopeptidase activity with POP. As well as being functionally related, the active sites of these three enzymes share a high structural identity, with conserved Arg, Phe and Tyr residues surrounding the catalytic Ser (Juillerat-Jeanneret, 2008). Thus, the design of inhibitors with a good degree of selectivity between these enzymes has proved difficult, and it is of utmost importance to avoid cross-reactivity and undesired side effects (Poplawski et al., 2013).

To assess the off-target reactivity of our compounds, three class-representative inhibitors (**8**, **13** and **18**) were screened against FAP and DPPIV, at concentrations up to 50 μM (~50,000-fold the POP IC_{50}). In this assay, a remarkable level of selectivity was found for all three families (Table S1). Even at the highest concentration of inhibitors (50 μM), catalytic activities > 70% were observed in all cases for FAP and DPPIV. In particular, inhibitor **18** had a marginal inhibitory effect (below 20%) on the closely related FAP protease. At lower concentrations—in the POP IC_{50} range—these compounds were able to fully discriminate between the different proline-specific peptidases. This high specificity fulfills a main requirement for the selective and covalent modulation of the POP enzyme.

Binding is fast, irreversible and specific for the catalytic Ser of POP

Considering the previous results, we selected inhibitor **18**—having a suitable pharmacological profile and a more innovative scaffold—for further characterization. First, we studied the inhibition mechanism of POP by the sulfonyl fluoride warhead. From a kinetic perspective, covalent drugs block their targets in a two-step fashion (Singh et al., 2011). Initially, the inhibitor associates via non-covalent interactions to the target enzyme—a process defined by K_i—and afterwards the nucleophilic attack by the protein takes place, giving rise to the inhibited complex—defined by k_2 (Figure 2B). In those cases in which the inhibition is effectively irreversible, k_{-2} will essentially be zero, and, if allowed sufficient time, the binding reaction will proceed to completion rather to equilibrium. In order to confirm that the inhibitory mechanism was irreversible, compound **18** was subjected to a complete kinetic profiling (Figure 2B).

In this experiment, an exponential decay in enzyme activity, dependent on the preincubation time, was observed, thus confirming the irreversible nature of POP inhibition. In the context of irreversible binding, inhibitor potency and selectivity can be governed by the initial non-covalent binding to the enzyme (K_i), by the subsequent bonding step (k_2), or by both of them (k_2/K_i). For compound **18**, the k_2/K_i ratio—being

the parameter that best represents inhibitory potency—was 2×10^6 M^{-1} s^{-1}, thus indicating a potent and fast inactivation of the enzyme (Miyahisa et al., 2015).

Additionally, mass spectrometry analysis of a BrCN-digested POP sample was performed to confirm the specific binding of **18** to the active site. In this assay, the mass of the peptide containing the catalytic Ser554 was increased by 508 Da, versus a buffer-treated reference sample, which indicated single sulfonylation of the Ser side chain, consistent with a 1:1 inhibitor/protein ratio (Figure 2C). Therefore, the combination of kinetic and mass spectrometry POP binding assays reinforced our initial assumption of covalent and irreversible modification of the enzyme through the prolylsulfonyl warhead.

Low-nanomolar POP inhibition in intact human cells

In order to assess the activity of our hit compound in a biologically more relevant environment, human neuroblastoma SH-SY5Y cells were treated with inhibitor **18** at concentrations ranging from 0.2 pM to 200 nM. Subsequently, POP activity was measured on intact cells by recording the release of fluorescence from a specific substrate (Z-Gly-Pro-AMC). Under these conditions, compound **18** was able to reach the cytosol and produce a fast—10-min incubation time—and strong inhibition of the POP enzyme, showing an IC_{50} of 1.4 nM (Figure 3B).

Collectively, our findings show how the distinct strengths of reversible and irreversible mechanisms can be combined to yield drug candidates with carefully tuned reactivity and specific target engagement. As pursued with the structure-based design, the optimal selection of P2-P3 groups, combined with a novel prolylsulfonyl fluoride warhead, yielded POP inhibitors that were not only highly potent and selective, but also CNS-permeable. By analogy with other covalent inhibitors such as ZPP, the binding of these compounds to the POP active site may produce a prolonged modulation of the highly dynamic protein conformational equilibrium, effectively stabilizing the closed or inactive state of the enzyme (López et al., 2016). If this was the case, our inhibitors would ultimately abolish the deleterious interactions of POP with pathogenic proteins such as α-synuclein, thus opening the door for new treatments of CNS pathologies.

Significance

POP is a proteolytic enzyme and partner in intracellular PPIs that is actively involved in the pathogenesis of several cognitive disorders ranging from Parkinson's disease to schizophrenia. Thus, designing efficient inhibitors able to reach the brain and discriminate POP from other proteases has been one of the main objectives of researchers in the field. However, most reported drugs are reversible inhibitors that have found limited *in vivo* application, mostly due to low membrane permeability, lack of selectivity and short residence times. Here, we report the design of shape-complementary targeted inhibitors that exert sustained POP inhibition at very low concentrations. In our bifunctional molecules, the peptide backbone and side chains form a template that selectively recognizes the active site of the enzyme—thus

providing selectivity—while the sulfonyl fluoride electrophile irreversibly binds to the catalytic Ser. In addition to their low-nM potency, these compounds were >1000x selective for POP over two closely related proteases (DPPIV and FAP), thus ensuring low cross-reactivity. Notably, high permeability values were obtained in both PAMPA and MDCK assays, a property that translates into a potent cellular activity, as it was shown in SH-SY5Y human cells. Beyond their application in the study of the function of POP in CNS disorders, these compounds pave the way for the design of selective irreversible inhibitors of other serine proteases.

Acknowledgements

This study was funded by MINECO-FEDER (BIO 2016-75327-R) and Generalitat de Catalunya (XRB and 2017SGR-998). We also thank the NMR facility from Scientific and Technological Centre of the University of Barcelona (CCiT UB), the Mass Spectrometry Core Facility (IRB Barcelona) and the Barcelona Supercomputing Center (BSC) for their technical support. IRB Barcelona is the recipient of a Severo Ochoa Award of Excellence from MINECO (Government of Spain).

Author contributions

S.G. wrote the manuscript, designed the research, performed the research and analyzed the data; R.P. wrote the manuscript, designed the research and analyzed the data; L.M. provided useful support for the *in vitro* studies; A. J. B. and J.S. performed the chemical synthesis and analyzed the data; L.N., T.T., R. M. J. L. and E.G. designed the research and supervised the experiments. All authors commented on the manuscript.

Declaration of interests

E.G., R.P. and T.T. have filed a patent (EP2917209B1). The other authors declare no competing interests.

References

Baillie, T.A. (2016). Targeted Covalent Inhibitors for Drug Design. Angew. Chemie Int. Ed. *55*, 13408–13421.

Brandt, I., Gérard, M., Sergeant, K., Devreese, B., Baekelandt, V., Augustyns, K., Scharpé, S., Engelborghs, Y., and Lambeir, A.-M. (2008). Prolyl oligopeptidase stimulates the aggregation of alpha-synuclein. Peptides *29*, 1472–1478.

Brouwer, A.J., Ceylan, T., Jonker, A.M., van der Linden, T., and Liskamp, R.M.J. (2011). Synthesis and biological evaluation of novel irreversible serine protease inhibitors using amino acid based sulfonyl fluorides as an electrophilic trap. Bioorg. Med. Chem. *19*, 2397–2406.

Checler, F., Vincent, J.P., and Kitabgi, P. (1985). Inactivation of Neurotensin by Rat Brain Synaptic Membranes Partly Occurs Through Cleavage at the Arg8 -Arg9 Peptide Bond by a Metalloendopeptidase. J. Neurochem. *45*, 1509–1513.

Di Daniel, E., Glover, C.P., Grot, E., Chan, M.K., Sanderson, T.H., White, J.H., Ellis, C.L.,

Gallagher, K.T., Uney, J., Thomas, J., et al. (2009). Prolyl oligopeptidase binds to GAP-43 and functions without its peptidase activity. Mol. Cell. Neurosci. *41*, 373–382.

Di, L., Kerns, E.H., Fan, K., McConnell, O.J., and Carter, G.T. (2003). High throughput artificial membrane permeability assay for blood-brain barrier. Eur. J. Med. Chem. *38*, 223–232.

Dubiella, C., Cui, H., Gersch, M., Brouwer, A.J., Sieber, S.A., Krüger, A., Liskamp, R.M.J., and Groll, M. (2014). Selective inhibition of the immunoproteasome by ligand-induced crosslinking of the active site. Angew. Chemie - Int. Ed. *53*, 11969–11973.

Fülöp, V., Böcskei, Z., and Polgár, L. (1998). Prolyl oligopeptidase: an unusual beta-propeller domain regulates proteolysis. Cell *94*, 161–170.

Giralt, E., Prades, R., Tarrago, T., and Royo, S. (2014). 1-[1-(benzoyl)-pyrrolidine-2-carbonyl]-pyrrolidine-2-carbonitrile derivatives.

Hannula, M.J., Myöhänen, T.T., Tenorio-Laranga, J., Männistö, P.T., and Garcia-Horsman, J.A. (2013). Prolyl oligopeptidase colocalizes with α-synuclein, β-amyloid, tau protein and astroglia in the post-mortem brain samples with Parkinson's and Alzheimer's diseases. Neuroscience *242*, 140–150.

Höfling, C., Kulesskaya, N., Jaako, K., Peltonen, I., Männistö, P.T., Nurmi, A., Vartiainen, N., Morawski, M., Zharkovsky, A., Võikar, V., et al. (2016). Deficiency of prolyl oligopeptidase in mice disturbs synaptic plasticity and reduces anxiety-like behaviour, body weight, and brain volume. Eur. Neuropsychopharmacol. *26*, 1048–1061.

Huhn, A.J., Guerra, R.M., Harvey, E.P., Bird, G.H., and Walensky, L.D. (2016). Selective Covalent Targeting of Anti-Apoptotic BFL-1 by Cysteine-Reactive Stapled Peptide Inhibitors. Cell Chem. Biol. *23*, 1123–1134.

Juillerat-Jeanneret, L. (2008). Prolyl-Specific Peptidases and Their Inhibitors in Biological Processes. Curr. Chem. Biol. *2*, 97–109.

Kaszuba, K., Róg, T., Danne, R., Canning, P., Fülöp, V., Juhász, T., Szeltner, Z., St. Pierre, J.-F., García-Horsman, A., Männistö, P.T., et al. (2012). Molecular dynamics, crystallography and mutagenesis studies on the substrate gating mechanism of prolyl oligopeptidase. Biochimie *94*, 1398–1411.

L'heureux, A., Beaulieu, F., Bennett, C., Bill, D.R., Clayton, S., Laflamme, F., Mirmehrabi, M., Tadayon, S., Tovell, D., and Couturier, M. (2010). Aminodifluorosulfinium salts: selective fluorination reagents with enhanced thermal stability and ease of handling. J. Org. Chem. *75*, 3401–3411.

Li, J., Wilk, E., and Wilk, S. (1996). Inhibition of prolyl oligopeptidase by Fmoc-aminoacylpyrrolidine-2-nitriles. J. Neurochem. *66*, 2105–2112.

López, A., Tarragó, T., and Giralt, E. (2011). Low molecular weight inhibitors of Prolyl Oligopeptidase: a review of compounds patented from 2003 to 2010. Expert Opin. Ther. Pat. *21*, 1023–1044.

López, A., Mendieta, L., Prades, R., Royo, S., Tarragó, T., and Giralt, E. (2013). Peptide POP inhibitors for the treatment of the cognitive symptoms of schizophrenia. Future

Med. Chem. *5*, 1509–1523.

López, A., Herranz-Trillo, F., Kotev, M., Gairí, M., Guallar, V., Bernadó, P., Millet, O., Tarragó, T., and Giralt, E. (2016). Active-Site-Directed Inhibitors of Prolyl Oligopeptidase Abolish Its Conformational Dynamics. ChemBioChem *17*, 913–917.

Mariaule, G., De Cesco, S., Airaghi, F., Kurian, J., Schiavini, P., Rocheleau, S., Huskić, I., Auclair, K., Mittermaier, A., and Moitessier, N. (2016). 3-Oxo-hexahydro-1H-isoindole-4-carboxylic Acid as a Drug Chiral Bicyclic Scaffold: Structure-Based Design and Preparation of Conformationally Constrained Covalent and Noncovalent Prolyl Oligopeptidase Inhibitors. J. Med. Chem. *59*, 4221–4234.

Miyahisa, I., Sameshima, T., and Hixon, M.S. (2015). Rapid Determination of the Specificity Constant of Irreversible Inhibitors (kinact/KI) by Means of an Endpoint Competition Assay. Angew. Chemie - Int. Ed. *54*, 14099–14102.

Narayanan, A., and Jones, L.H. (2015). Sulfonyl fluorides as privileged warheads in chemical biology. Chem. Sci. *6*, 2650–2659.

Pardridge, W.M. (2005). The blood-brain barrier: bottleneck in brain drug development. NeuroRx *2*, 3–14.

Poplawski, S.E., Lai, J.H., Li, Y., Jin, Z., Liu, Y., Wu, W., Wu, Y., Zhou, Y., Sudmeier, J.L., Sanford, D.G., et al. (2013). Identification of selective and potent inhibitors of fibroblast activation protein and prolyl oligopeptidase. J. Med. Chem. *56*, 3467–3477.

Prades, R., Munarriz-Cuezva, E., Urigüen, L., Gil-Pisa, I., Gómez, L., Mendieta, L., Royo, S., Giralt, E., Tarragó, T., and Meana, J.J. (2017). The prolyl oligopeptidase inhibitor IPR19 ameliorates cognitive deficits in mouse models of schizophrenia. Eur. Neuropsychopharmacol. *27*, 180–191.

Savolainen, M.H., Yan, X., Myöhänen, T.T., and Huttunen, H.J. (2015). Prolyl oligopeptidase enhances α-synuclein dimerization via direct protein-protein interaction. J. Biol. Chem. *290*, 5117–5126.

Schechter, I., and Berger, A. (1967). On the size of the active site in proteases. I. Papain. Biochem. Biophys. Res. Commun. *27*, 157–162.

Singh, J., Petter, R.C., Baillie, T.A., and Whitty, A. (2011). The resurgence of covalent drugs. Nat. Rev. Drug Discov. *10*, 307–317.

Svarcbahs, R., Julku, U.H., and Myöhänen, T.T. (2016). Inhibition of Prolyl Oligopeptidase Restores Spontaneous Motor Behavior in the α-Synuclein Virus Vector–Based Parkinson's Disease Mouse Model by Decreasing α-Synuclein Oligomeric Species in Mouse Brain. J. Neurosci. *36*.

Tarrago, T., Kichik, N., Seguí, J., and Giralt, E. (2007). The Natural Product Berberine is a Human Prolyl Oligopeptidase Inhibitor. ChemMedChem *2*, 354–359.

Tarragó, T., Frutos, S., Rodriguez-Mias, R.A., and Giralt, E. (2006). Identification by 19F NMR of Traditional Chinese Medicinal Plants Possessing Prolyl Oligopeptidase Inhibitory Activity. ChemBioChem *7*, 827–833.

Toide, K., Iwamoto, Y., Fujiwara, T., and Abe, H. (1995). JTP-4819: a novel prolyl

endopeptidase inhibitor with potential as a cognitive enhancer. J. Pharmacol. Exp. Ther. *274*.

Tschan, S., Brouwer, A.J., Werkhoven, P.R., Jonker, A.M., Wagner, L., Knittel, S., Aminake, M.N., Pradel, G., Joanny, F., Liskamp, R.M.J., et al. (2013). Broad-spectrum antimalarial activity of peptido sulfonyl fluorides, a new class of proteasome inhibitors. Antimicrob. Agents Chemother. *57*, 3576–3584.

Venäläinen, J.I., Garcia-Horsman, J.A., Forsberg, M.M., Jalkanen, A., Wallén, E.A.A., Jarho, E.M., Christiaans, J.A.M., Gynther, J., and Männistö, P.T. (2006). Binding kinetics and duration of in vivo action of novel prolyl oligopeptidase inhibitors. Biochem. Pharmacol. *71*, 683–692.

Wang, Q., Rager, J.D., Weinstein, K., Kardos, P.S., Dobson, G.L., Li, J., and Hidalgo, I.J. (2005). Evaluation of the MDR-MDCK cell line as a permeability screen for the blood–brain barrier. Int. J. Pharm. *288*, 349–359.

Yoshimoto, T., Nishimura, T., Kita, T., and Tsuru, D. (1983). Post-proline cleaving enzyme (prolyl endopeptidase) from bovine brain. J. Biochem. *94*, 1179–1190.

Yoshimoto, T., Kawahara, K., Matsubara, F., Kado, K., and Tsuru, D. (1985). Comparison of inhibitory effects of prolinal-containing peptide derivatives on prolyl endopeptidases from bovine brain and Flavobacterium. J. Biochem. *98*, 975–979.

Figure legends

Figure 1. Structure-guided design of irreversible POP inhibitors. A) Crystal structure of KYP-2047 bound to the POP active site (PDB 4an0), highlighting the main enzyme cavities (S1, S2 and S3) and contiguous residues. B) Representative examples of covalent POP inhibitors. C) General structure of the family of shape-complementary POP inhibitors. Selected P2 and P3 groups are combined with a sulfonyl fluoride electrophile to generate irreversible-binding peptidomimetics.

Figure 2. Sulfonyl fluoride peptidomimetics show high BBB permeability and specific and irreversible binding to the POP catalytic site. A) Apparent permeability (P_{app}) of compounds **7**-**20** and metoprolol (control) in MDCK cells. Error bars represent standard deviations of triplicate samples. B) Kinetic constants that define a covalent binding process (top). The exponential decay of POP activity, at several concentrations of inhibitor **18**, is represented versus the pre-incubation time (left). The k_{obs} plot (right) yields the kinetic parameters that govern irreversible binding (K_i, k_2). C) Mass spectra (right) and deconvoluted mass (left) of the CNBr-digested catalytic peptide of POP, showing selective covalent modification of Ser554 by **18**.

Figure 3. Inhibitor 18 covalently binds to the POP catalytic site and displays low-nanomolar activity in human cells. A) A) Predicted binding of inhibitor **18** (structure shown bottom right) to the POP catalytic pocket, highlighting the main cavities (S1, S2 and S3) and interacting residues. Hydrogen bonds are shown with yellow dashes. B) POP activity in intact human SH-SY5Y cells at different concentrations of **18**. Error bars represent standard deviations of triplicate samples.

Tables

Table 1. Structure of designed POP inhibitors, their activity and permeability profile.

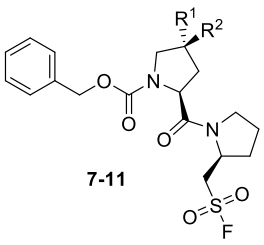

7-11

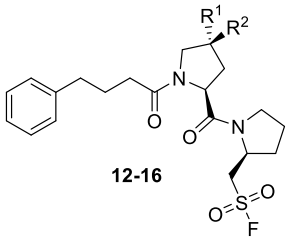

12-16

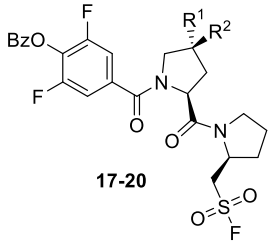

17-20

Id	R^1	R^2	Yield (%)[a]	POP IC_{50} (nM)	Transport (%)[b]	Retention (%)[b]	P_e (10^{-6} cm s^{-1})[b]
7	H	H	75	1.3	19.1	37.1	11.4
8	F	H	51	4.5	18.8	19.7	11.2
9	F	F	41	21.2	24.8	2.1	16.3
10	H	CF_3	48	7.9	14.0	40.7	7.8
11	H	CH_3	62	0.8	23.9	14.2	15.4
12	H	H	59	3.2	21.5	29.3	13.3
13	F	H	43	1.9	20.2	23.6	12.2
14	F	F	28	2.3	25.4	20.4	16.8
15	H	CF_3	40	2.1	21.5	51.2	13.3
16	H	CH_3	46	1.9	20.3	57.8	12.4
17	H	H	39	1.8	25.4	26.7	17.2
18	F	H	26	0.9	26.5	34.0	17.9
19	F	F	18	1.7	15.3	62.3	8.7
20	H	CH_3	33	1.2	19.6	51.4	11.8
KYP-2047				3.9	13.3	0.6	7.3

[a]Isolated yields of the coupling reactions. [b]Transport, retention and permeability parameters obtained in the PAMPA assay. Data represent mean values (n=3).

Contact for reagent and resource sharing

Further information and requests for resources and reagents should be directed to and will be fulfilled by the Lead Contact, Ernest Giralt (ernest.giralt@irbbarcelona.org)

Experimental model and subject details

Human SH-SY5Y cells were obtained from the American Type Culture Collection (ATCC). Cells were cultured in DMEM-high-glucose medium containing 10% fetal bovine serum (FBS), 1% glutamine and 1% penicillin-streptomycin and grown in a humidified incubator at 37ºC, 5% CO2.

Method details

General

Unless otherwise stated, all solvents and chemicals were used as received. All solvent mixtures (eluents) are given in v/v.

Analytical and preparative HPLC

All reactions were monitored by HPLC (Waters Alliance 2695 equipped with 2487 photodiode array detector, Sunfire C18 column (2.1 x 1000 mm, 3.5 µm, 100 Å, Waters); flow rate = 1 mL/min; solvents A=0.036% trifluoroacetic acid in water, and B=0.045% trifluoroacetic acid in acetonitrile. The reaction crude products were purified by semi-preparative HPLC on a Waters 2700 sample manager equipped with a Waters 2487 dual wavelength absorbance detector, a Waters 600 controller, a Waters fraction collector; using a symmetry C18 column (100 mm x 19 mm, 5 µm; Waters). Column flow was set at 15 ml/min; solvents A=0.1% trifluoroacetic acid in water, and B=0.1% trifluoroacetic acid in acetonitrile. The purity of all final compounds was 95% or higher, as measured by HPLC.

TLC

Reactions for compounds **5**-**10** were monitored by TLC analysis using Merck pre-coated silica gel 60 F-254 (0.25 mm) plates. Spots were visualized with UV light, ninhydrin, Cl2-TDM or sulfuric acid. Solvents were evaporated under reduced pressure at 40°C. Column chromatography was performed on Siliaflash P60 (40-63 µm) from Silicycle (Canada).

NMR

NMR spectra were recorded on Varian Mercury 400, Agilent 400, or Varian Inova 500 MHz spectrometers, using $CDCl_3$ as solvent at 25°C. Variable temperature ^{1}H NMR spectra (400 MHz) were recorded on a Varian S400 spectrometer. Chemical shifts are given in parts per million (ppm) (δ relative to residual solvent peak for ^{1}H and ^{13}C, or relative to TMS (0.00 ppm) for compounds **5**-**10**). Some of the ^{13}C NMR spectra were recorded using the attached proton test (apt) pulse sequence. Most of the ^{1}H and ^{13}C NMR spectra contained additional peaks, due to the presence of rotamers and fluorine atoms.

Chemical syntheses

Synthesis of the prolylsulfonyl fluoride electrophile (6)

Cbz-Pro-ψ[CH_2S]-Ac (2). To a solution of Cbz-Prolinol (**1**, 51.8 g, 220 mmol) in CH_2Cl_2 (1.0 L) was added Et_3N (36.8 ml, 262 mmol) and the resulting solution was cooled in an icebath for 1 h under N_2 atmosphere. Methanesulfonyl chloride (20.4 ml, 264 mmol) was added dropwise and the mixture was stirred overnight at r.t. Additional CH_2Cl_2 (1.0 L) was added and the mixture was washed with $KHSO_4$ (1.0 M, 3 x 1.0 L), water (1.0 L) and brine. The organic layer was dried with Na_2SO_4 and concentrated *in vacuo*, affording the mesylate as a yellow oil (69.6 g, 220 mmol, quantitative). The mesylate was not stored, but used directly in the reaction with *in situ* generated cesium thioacetate. To this end, thioacetic acid (23.4 mL, 332 mmol, 1.5 eq.) was added to a mixture of cesium carbonate (53.3 g, 164 mmol) in DMF (1.1 L) under N_2 atmosphere. After stirring for 5 min, the resulting suspension was decanted to the mesylate. The flask was covered with aluminium foil and the mixture was stirred over 3 nights at r.t. After completion, EtOAc (2.5 L) and water (1.0 L) were added and the water layer was extracted with EtOAc (0.5 L). The combined organic layer was washed with saturated $NaHCO_3$ solution (1.0 L, 2x), $KHSO_4$ (1.0 M, 1.0 L, 2x) and brine (300 ml). After drying (Na_2SO_4) and concentration *in vacuo*, the crude product was purified by column chromatography (EtOAc: Hex, 1:9), affording **3** as a yellowish solid (43.9 g, 150 mmol, 68%).

Cbz-Pro-ψ[CH_2SO_2]-ONa (3). To a solution of thioacetate **2** (43.9 g, 150 mmol) in acetic acid (450 mL) was added an aqueous hydrogen peroxide solution (150 mL, 30% w/w) and the mixture was stirred overnight at r.t. The color of the reaction changed overnight from clear brown to clear yellow. $NaOAc.3H_2O$ (20.4 g, 150 mmol) was added and stirring was continued for 15 min. DMF (500 mL) was added and the solution was concentrated *in vacuo* to approximately half of its volume. Another portion of DMF (500 mL) was added and evaporated again to about one third of the volume. The addition and evaporation of DMF was repeated until no more peroxide was detected in the receiver flask with KI/starch paper. The mixture was then concentrated completely, and water (1.0 L) and CH_2Cl_2 (500 mL) were added, after which the aqueous layer was washed once with CH_2Cl_2 (500 mL). Lyophilization of the water layer afforded **3** as a white solid (47.6 g, 145 mmol, 97%).

Cbz-Pro-ψ[CH_2SO_2]-F (5). To a suspension of Cbz-Pro-ψ[CH_2SO_2]-ONa (**3**, 9.64 g, 30 mmol) in CH_2Cl_2 (600 mL) was added was XtalFluor-M (**7**, 13.2 g, 54.3 mmol), under N_2 atmosphere. After addition of $Et_3N.3HF$ (212 µL, 1.30 mmol), the mixture was refluxed for 17 h with the condenser fitted with a drying tube. Unreacted XtalFluor-M was quenched by addition of silica gel (approximately 20 g) and stirring for 5 min. After filtration, the mixture was concentrated *in vacuo* and re-dissolved in EtOAc (400 mL) and water (100 mL). After separation, the organic layer was directly dried (Na_2SO_4), concentrated to dryness, and loaded (dissolved in CH_2Cl_2) on a silica gel column. After elution (eluent: CH_2Cl_2) using slight pressure (balloon), sulfonyl fluoride **5** was obtained as a white solid (6.89 g, 22.9 mmol, 76%).

HCl.H-Pro-ψ[CH_2SO_2]-F (6). To a solution of sulfonyl fluoride **5** (6.89 g, 22.9 mmol) in dichloromethane (230 mL) was added a solution of HBr in acetic acid (33%, 138 mL). After stirring at r.t. for 30 min, the solvents were removed *in vacuo*. The residue was dissolved in H_2O (230 mL) and washed with EtOAc (2 x 200 mL). Dowex 2x8 (13.8 g, Cl-form) was then added. After stirring for 5 min at r.t., the resin was filtered off. Lyophilization of the filtrate afforded HCl-salt **6** as an off-white solid (4.2 g, 20.6 mmol, 90%).

Synthesis of the final POP inhibitors

General Procedure for the Synthesis of Intermediates 23-27. Benzylchloroformate (1.1 eq., 0.13 mmol) was added dropwise to a stirred solution of the corresponding proline analog (1 eq., 0.12 mmol) and $NaHCO_3$ (2.5 eq., 0.3 mmol) in water/THF (1:1, 1 mL) at 0°C. The reaction was stirred for 30 min at 0°C and for 5 h at r.t. The solution was acidified with 1M HCl aqueous solution and extracted with AcOEt (3 x 10 mL). The combined organic layer was washed with brine (20 mL), dried over $MgSO_4$, filtered, and evaporated. Crude products were used in the next step without further purification.

General Procedure for the Synthesis of Intermediates 28-36. 4-(benzyloxy)-3,5-difluorobenzoic acid was obtained as previously described (Giralt et al., 2014). 4-phenylbutanoic acid or 4-(benzyloxy)-3,5-difluorobenzoic acid (1 eq., 0.12 mmol) were stirred at r.t. in anhydrous toluene (1 mL) for 10 min. Oxalyl chloride (1.5 eq., 0.18 mmol) was added, and the reaction was stirred at 50°C for 1.5 h. The solvent was removed *in vacuo* and the resulting crude product was redissolved in anhydrous THF. DIPEA (2 eq., 41.8 µL) and the corresponding proline (1 eq., 0.12 mmol) was added neat at 0°C. The reaction was stirred at 0°C for 1 h and at r.t. for 3 h. The mixture was concentrated *in vacuo*, redissolved in water (3 mL), and acidified with 1M HCl aqueous solution. The aqueous solution was extracted with AcOEt (3 x 10 mL); the combined organic layer was washed with brine (20 mL), dried over $MgSO_4$, filtered, and evaporated. Crude products were used in the next step without further purification.

General Procedure for L-prolylmethanesulfonyl Fluoride Coupling. HATU (1.1 eq., 0.13 mmol) and DIPEA (2 eq., 0.24 mmol) were added to a solution of the corresponding intermediate **23**-**36** (1 eq., 0.12 mmol) in DCM (1 mL). After 5 min, neat (S)-pyrrolidin-2-ylmethanesulfonyl fluoride (HCl salt **6** or TFA salt **22**) was added, and the mixture was stirred for 3 h at r.t. The reaction mixture was diluted with DCM (10 mL), and 5% $KHCO_3$ aqueous solution was added (10 mL). The organic layer was then dried over $MgSO_4$, filtered, and evaporated *in vacuo*. The crude product was redissolved in 2:8 water/acetonitrile and purified by semi-preparative HPLC.

Covalent docking of the POP inhibitors

In order to assess the potential binding of our compounds to POP and to study the key interactions within the catalytic site, we applied the docking software CovDock to predict the position of covalently bound **18** in the POP active site. As no crystal structure of human POP has been elucidated to date, porcine POP, which shares 97%

identity with the human form, was used for the docking experiment (PDB code: 2XDW). After docking, a short minimization of the complex was performed, and the top 20 results were ranked. In its lowest energy conformation, **18** adopted a very similar conformation to that reported for ligands ZPP and KYP-2047 co-crystalized with POP.

POP activity assays

POP was obtained by expression in E. coli and affinity purification as reported previously (Tarragó et al., 2006). POP activity was determined following the method described by Toide and coworkers (Toide et al., 1995). The reactions were performed in 96-well microplates, thereby allowing the simultaneous monitoring of multiple reactions. For each reaction, the activity buffer (137 µL, 100 mM of Na/K phosphate buffer, pH 8.0) was pre-incubated for 15 min at 37ºC with POP (5 nM) and with the corresponding inhibitor solution (3 µL). Stock solutions at a range of inhibitor concentrations (typically 1 nM to 5 mM) were prepared in DMSO. After pre-incubation, ZGP-AMC (N-benzyloxycarbonyl-Gly-Pro-methylcoumarinyl-7-amide, 10 µL, 450 µM in 40% of 1,4-dioxane) was added, and the reaction was monitored at the fluorimeter at 37ºC . The formation of AMC was measured fluorimetrically (excitation and emission wavelengths were 360/40 and 485/20 nm, respectively). For each sample, a negative control containing 3 µL of the sample in DMSO, 10 µL of ZGP-AMC solution and 137 µL of activity buffer were added into the well plate. The positive control of the reaction consisted of 3 µL of DMSO, 10 µL of ZGP-AMC solution and 137 µL of 5 nM POP in activity buffer.

For the kinetic determination of compound **18**, the same methodology was applied using a range of inhibitor concentrations (1 to 100 nM) and several preincubation times (0 to 60 min). Then, fluorogenic substrate ZGP-AMC was added and fluorescence was read after 30 minutes. The fitting of the data and calculation of the kinetic parameters was performed as shown in Figure 2.

Mass spectrometry assays

Exact mass determination was performed on a LTQ-FT Ultra instrument (Thermo Scientific) by direct infusion of sample (1 µM concentration in 1:1 water/acetonitrile, 0.1% formic acid) through a nanoESI chip; detection method scan (150-2000 a.m.u. range).

For the detection of inhibitor **18** bound to the catalytic site, a POP sample (130 µL, 20 µM in 100 mM of Na/K phosphate buffer, pH 8.0) was incubated with 3 equivalents of **18** at 25ºC during 1 h. The sample was lyophilized, resuspended in 100 µL of water containing 40% formic acid and 0.25 M cyanogen bromide and digested in darkness for 16 h at 25ºC. Samples were desalted on a PolyLC C4 column and eluted with 95% acetonitrile in 1% formic acid. The samples were dried in a vacuum centrifuge and reconstituted in 50 µL of water/acetonitrile (1:1) containing 1% formic acid, and were directly infused on an LTQ-FT Ultra instrument (Thermo Scientific).

Cell activity assays

Human SH-SY5Y cells (on passage 15) were seeded (5000 cells per well) in a fluorescence 96-well plate suitable for cell culture. After 72 h of incubation at 37ºC, cells reached 90-100% confluence. Cells were washed with PBS and treated with different concentrations of compound **18** (0.2 to 200 nM) in 140 µL of PBS. After 10 min of pre-incubation time, ZGP-AMC (10 µL, 150 µM in 40% of 1,4-dioxane) was added, and the reaction was monitored at the fluorimeter at 37ºC. The formation of AMC was measured fluorimetrically (excitation and emission wavelengths were 360/40 and 485/20 nm, respectively). Triplicates for each concentration, as well as blanks, were included. Fluorescence values during the linear time of the inhibition (typically, 30 min) were determined and the IC50 values were then calculated.

Selectivity versus FAP

To determine the activity of FAP in the presence of the inhibitors, reactions were performed in 96-well microplates. For each reaction, the activity buffer (129.5 µL, 100 mM of Na/K phosphate buffer, pH 8.0) was pre-incubated for 15 min at 37ºC with recombinant human FAP (7.5 µL, 0.57 nM) and with the corresponding inhibitor solution (3 µL). Stock solutions at a range of inhibitor concentrations were prepared in DMSO. After pre-incubation, ZGP-AMC (10 µL, 1.5 mM in 40% of 1,4-dioxane) was added, and the reaction was incubated for 60 min at 37ºC in a fluorimeter. The formation of AMC was monitored fluorimetrically (excitation and emission wavelengths were 360/40 and 485/20 nm, respectively). For each sample, a negative control containing 3 µL of the sample in DMSO, 10 µL of ZGP-AMC solution, and 129.5 µL of activity buffer were added to the well plate. The positive control of the reaction consisted of 3 µL of DMSO, 10 µL of ZGP-AMC solution, and 137 µL of 0.57 nM FAP in activity buffer. Triplicates for each condition were included. Fluorescence values versus time were represented and the lineal time was determined. Afterwards, the percentage of FAP inhibition was calculated at point concentrations of inhibitors (50, 10, 5 and 1 µM) by comparing the fluorescence intensity of the sample with that of the blank.

Selectivity versus DPPIV

The ectodomain (residues 39-766) of dipeptidyl peptidase-IV (DPPIV) was obtained by expression in Sf9 insect cells using the Baculovirus technique. DPPIV activity was determined following the method previously described (Checler et al., 1985). The reactions were performed in 96-well microplates. For each reaction, the activity buffer (132 µL, 50 mM Tris, 1 M NaCl, 1 mg/mL BSA, pH 7.5) was pre-incubated for 15 min at 37ºC with recombinant human DPPIV (5 µL, 12.3 µg/mL) and with the corresponding inhibitor solution (3 µL). Stock solutions at a range of inhibitor concentrations were prepared in DMSO. After pre-incubation, GP-AMC (H-Gly-Pro-methylcoumarinyl-7-amide, 10 µL, 0.75 mM in 40% of 1,4-dioxane) was added, and the reaction was incubated for 20 min at 37ºC. The formation of AMC was monitored fluorimetrically every 5 min (excitation and emission wavelengths were 360/40 and 485/20 nm,

respectively). For each sample, a negative control containing 3 µL of the sample in DMSO, 10 µL of GP-AMC solution and 132 µL of activity buffer were added to the well plate. The positive control of the reaction consisted of 3 µL of DMSO, 10 µL of GP-AMC solution and 132 µL of 12.3 µg/mL DPPIV in activity buffer. Triplicates for each condition were included. Fluorescence values versus time were represented and the lineal time was determined. Afterwards, the percentage of DPPIV inhibition was calculated at point concentrations of inhibitors (50, 10, 5 and 1 µM) by comparing the fluorescence intensity of the sample with that of the blank.

Parallel Artificial Membrane Permeability Assay (PAMPA)

The PAMPA was used to determine the capacity of the compounds to cross the BBB by passive diffusion. The effective permeability of the compounds was measured at an initial concentration of 200 µM. The PAMPA buffer solution was prepared from a concentrated one and the pH was adjusted to 6.8. 1-propanol (20%) was added as a cosolvent to the buffer solution. Stock solutions of all compounds at 20 mM concentration were prepared in DMSO, and 1:100 dilution with PAMPA buffer was performed in each case. For the assays, the PAMPA sandwich was disenabled, and the donor wells were filled with 200 µL of the compound solution of interest. Before this, the polycarbonate filter of the membrane was coated with 4 µL of the commercial mixture of phospholipids. The acceptor compartments were filled with PAMPA buffer containing 1% DMSO (200 µL). After this, both plates were reassembled. The PAMPA sandwich was incubated in humidity-saturated chamber for 4 h with orbital agitation at 100 rpm. After this time, the donor and acceptor wells were analyzed and quantified by HPLC at λ=220 nm. Propranolol was used as a positive control. Experiments were performed in triplicate. The phospholipid mixture used was a porcine polar brain lipid extract. Composition: phosphatidylcholine (PC) 12.6%, phosphatidylethanolamine (PE) 33.1%, phosphatidylserine (PS) 18.5%, phosphatidylinositol (PI) 4.1%, phosphatidic acid 0.8%, and 30.9% of other compounds. After 4 h, the effective permeability (P_e), the standard parameter that quantifies transport independently of time and concentrations, was calculated:

$$P_e = \frac{-218.3}{t} \log\left[1 - \frac{2C_A(t)}{C_D(t_o)}\right] \text{ x } 10^{-6}$$

where t is the running time (4 h), $C_A(t)$ is the concentration of compound in the acceptor well at time t and $C_D(t_0)$ is the concentration of compound in the donor well at t=0 h. Transport (%) values were obtained by dividing the amount in the acceptor well at time t, $C_A(t)$, by the amount in the donor well at time zero, $C_D(t_0)$, multiplied by 100. Permeability was considered excellent when values were >4.0 × 10^{-6} cm/s, uncertain between 2.0 × 10^{-6} and 4.0 × 10^{-6} cm/s, and poor below 2.0 × 10^{-6} cm/s (Di et al., 2003).

MDCK permeability assay

A monolayer of MDCK cells, already prepared in a 96-well plate, was purchased from ReadyCell, S.L. The Trans-Epithelial Electrical Resistance (TEER) was measured prior to

the assay in order to verify the integrity of the monolayer. Stock solutions of all compounds at 4 mM concentration were prepared in DMSO, and 1:100 dilutions with sterile HBSS buffer (supplemented with 5 mM glucose, pH 7) were performed in each case. Apical (donor) wells were filled with 100 µL of the compound solution (40 µM). Basal (acceptor) compartments were filled with PAMPA buffer containing 1% DMSO (250 µL). Then, both plates were reassembled and the multi-well plate was incubated for 2h at 37ºC. After this time, the donor and acceptor wells were disassembled and each analyzed by UPLC-MS. Metoprolol was used as a positive control. A Lucifer Yellow paracellular permeability assay was performed after the assay for quality control. All experiments were performed in triplicate. The apparent permeability for each compound was calculated using the following equation:

$$P_{\mathrm{app}} = \frac{dQ/dt}{C_o \,\mathrm{x}\, \mathrm{A}}$$

Data S1. NMR spectra and mass spectrometry characterization of the described final compounds and intermediates (related to Table 1).

Quantification and statistical analysis

In vitro experiments (Figure 2, 3 and S2) were performed in triplicate. For the enzyme activity and cellular assays, fluorescence values versus time were plotted and the lineal time was identified. Afterwards, the percentage of inhibition at each concentration was calculated and the results were fitted using a four parameter log[inhibitor] versus response and reported directly from the GraphPad Prism output.